Nonlinear atom optics and bright-gap-soliton generation in finite optical lattices

Iacopo Carusotto*
Laboratoire Kastler Brossel, École Normale Supérieure, 24 Rue Lhomond, 75231 Paris Cedex 05, France
and INFM, Scuola Normale Superiore, Piazza dei Cavalieri 7, I-56126 Pisa, Italy

Davide Embriaco
Dipartimento di Chimica Fisica ed Inorganica, Viale del Risorgimento 4, I-40136 Bologna, Italy
and INFM, Dipartimento di Fisica, Università di Pisa, I-56127 Pisa, Italy

Giuseppe C. La Rocca
Scuola Normale Superiore, Piazza dei Cavalieri 7, I-56126 Pisa, Italy
and INFM, Scuola Normale Superiore, Piazza dei Cavalieri 7, I-56126 Pisa, Italy
(Received 16 November 2001; revised manuscript received 16 January 2002; published 7 May 2002)

We theoretically investigate the transmission dynamics of coherent matter wave pulses across finite optical lattices in both the linear and the nonlinear regimes. The shape and the intensity of the transmitted pulse are found to strongly depend on the parameters of the incident pulse, in particular its velocity and density: a clear physical picture of the main features observed in the numerical simulations is given in terms of the atomic band dispersion in the periodic potential of the optical lattice. Signatures of nonlinear effects due to the atom-atom interaction are discussed in detail, such as atom-optical limiting and atom-optical bistability. For positive scattering lengths, matter waves propagating close to the top of the valence band are shown to be subject to modulational instability. A scheme for the experimental generation of narrow bright gap solitons from a wide Bose-Einstein condensate is proposed: the modulational instability is seeded starting from the strongly modulated density profile of a standing matter wave and the solitonic nature of the generated pulses is checked from their shape and their collisional properties.

DOI: 10.1103/PhysRevA.65.053611 PACS number(s): 03.75.Fi, 42.50.Vk, 42.65.−k

I. INTRODUCTION

In recent years, great interest has been devoted to theoretical as well as experimental studies of the propagation of matter waves in the periodic potential of optical lattices. The first experiments were carried out using ultracold atomic samples [1]; later on, the realization of atomic Bose-Einstein condensates (BECs) [2] and their coherent loading into optical lattices [3] opened the possibility of investigating features that follow from the coherent nature of the Bose-condensed atomic sample [4,5].

At the same time, the propagation of light waves in linear and nonlinear periodic dielectric structures has been a very active field of research: global photonic band gaps have been observed [6] and one-dimensional nonlinear periodic systems such as nonlinear Bragg fibers [7] are actually under intense investigation given the wealth of different phenomena including optical bistability, modulational instability, and solitonic propagation that can be observed [8–10].

Given the very close analogy between the behavior of coherent matter waves and nonlinear optics, we expect that the concepts currently used to study the physics of nonlinear Bragg fibers can be fruitfully extended to the physics of coherent matter waves in optical lattices: the optical potential of the lattice plays the role of the periodic refractive index, the atom-atom interactions are the atom-optical analog of a Kerr-like nonlinear refractive index, and the Gross-Pitaevskii equation of mean-field theory corresponds to Maxwell's equation with a nonlinear polarization term [11].

In the present paper, we shall report a theoretical investigation of the transmission dynamics of coherent matter pulses which are incident on a finite optical lattice with a velocity of the order of the Bragg velocity. In this velocity range, Bragg reflection processes are most effective and the atomic dispersion in the lattice is completely different from that in free space. Depending on the value of the density and the spatial size and velocity of the incident atomic cloud, as well as on the depth and length of the lattice, a number of different behaviors are predicted by numerical simulations; here, we shall focus our attention on the shape of the transmitted pulse just after it has crossed the lattice as well as while it is still propagating in the lattice. In particular, we shall discuss a mechanism that can be used to generate narrow bright atomic-gap solitons propagating along the lattice starting from a wide incident Bose-Einstein condensate. For more details of the continuous-wave transmission and reflection spectra in the linear regime, the reader can refer to [12–16]; some aspects of the linear pulse dynamics are discussed in [15].

The geometry considered in the present paper as well as in [12–16] is significantly different from the one usually considered in recent experimental work [3] on BEC dynamics in optical lattices, in which an optical lattice is switched on and superimposed on a stationary condensate; the dynamics of the condensate inside the lattice is then studied in response to some external force such as gravity, an acceleration of the lattice, or a spatial translation of the magnetic potential.

*Electronic address: Iacopo.Carusotto@lkb.ens.fr

The present paper is organized as follows. Section II describes the physical system under examination. In Sec. III we review some basic concepts of the dispersion of matter waves in the periodic potential of an infinite optical lattice and present some simple analytical calculations which accurately reproduce the dispersion of the atomic bands in the neighborhood of the first forbidden gap. The linear regime propagation of coherent matter wave pulses across finite lattices is the subject of Sec. IV. The intensity as well as the shape of the transmitted pulse are found to strongly depend on the properties of the weak incident pulse, in particular its velocity and spatial size; a simple interpretation of the observed phenomena in terms of allowed bands and forbidden gaps is provided. In Sec. V, we discuss the effect of atom-atom interactions on the propagation of the pulse in the different cases: simple explanations for the observed behavior are put forward in terms of familiar concepts of nonlinear optics such as optical limiting, optical bistability, or modulational instability; in the case of a positive scattering length, a broad pulse of matter waves propagating at the top of the valence band where the effective mass is negative is in fact subject to a dynamical instability (the so-called modulational instability) toward the formation of a train of narrow pulses as a consequence of the effective attractive interactions. In Sec. VI, we propose a scheme to exploit the modulational instability of valence band atoms in order to obtain a narrow bright gap soliton from a wide condensate: as an initial seed for the instability, the standing matter wave pattern created by the interference of the incident and reflected waves is used. The solitonic nature of the generated pulses is verified by looking at their dynamical and collisional properties as well as by comparing the pulse shape with the analytical predictions of the envelope-function approximation discussed in Sec. VII. Conclusions are finally drawn in Sec. VIII.

II. THE PHYSICAL SYSTEM

We consider a Bose-condensed atomic cloud in a quasi-one-dimensional (quasi-1D) geometry in which the transverse motion is frozen by the confining potential of an optical or magnetic atomic waveguide [17]. Gravity is made immaterial either by placing the waveguide axis along the horizontal plane or by counterbalancing the gravitational field with a suitable magnetic field gradient.

A periodic potential is created along the waveguide axis by means of a pair of far-off-resonance laser beams of frequency ω_L and wave vector $k_L=\omega_L/c$ crossing the waveguide at an angle θ as in Fig. 1 [3]: denoting by $\Omega_L(z)=|\vec{d}\cdot\vec{E}(z)|/\hbar$ the (slowly varying) single-beam Rabi frequency and with ω_{at} the atomic transition frequency, the optical potential experienced by the atoms is given by $V_{opt}(z)=V_0(z)\cos^2 k_{Br}z$, with $V_0(z)=\hbar\Omega_L(z)^2/(\omega_L-\omega_{at})$ and $k_{Br}=k_L\cos\theta$. For a red- or blue-detuned laser field, the optical potential is, respectively, attractive or repulsive; the lattice period $l_{Br}=\pi/k_{Br}$ can be tuned by varying the angle θ. The longitudinal envelope $V_0(z)$ of the lattice potential is determined by the profile of the laser beam waist and is assumed to smoothly vary on a length scale significantly longer than the lattice period l_{Br}. Unless differently specified, $V_0(z)$ will be taken as a Gaussian,

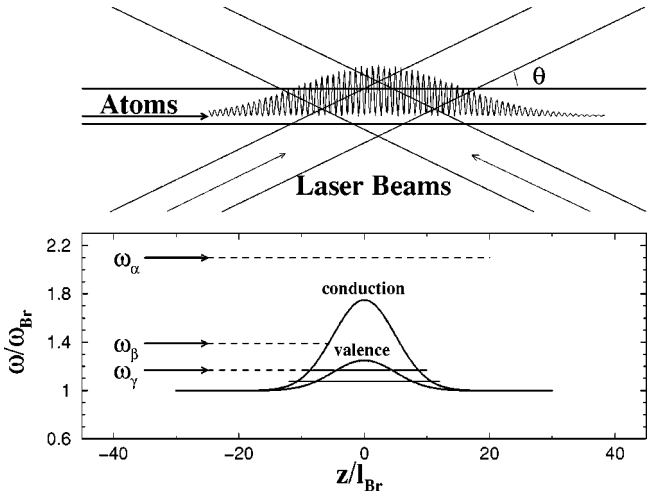

FIG. 1. Upper panel: schematic plot of the experimental setup under consideration. Lower panel: spatial dependence of the local band edge energies.

$$V_0(z)=V_0 e^{-z^2/2w_l^2}, \tag{1}$$

of height V_0 and spatial length w_l; for the sake of completeness, we have however verified that most of the qualitative features discussed in the present paper do not depend on the specific shape chosen for the longitudinal lattice envelope $V_0(z)$.

If both the kinetic and the interaction energy are much smaller than the transverse level spacing of the waveguide, this latter can be considered as being a single-mode one and the condensate wave function can be written in the factorized form

$$\psi(\mathbf{x})=\psi(z)\psi_\perp(\mathbf{x}_\perp), \tag{2}$$

where $\psi_\perp(\mathbf{x}_\perp)$ is the ground-state eigenfunction of the transverse confining potential with the appropriate $\int d^2\mathbf{x}_\perp|\psi_\perp(\mathbf{x}_\perp)|^2=1$ normalization. Within this approximation, the dynamics of the condensed atomic cloud can be described by a one-dimensional Gross-Pitaevskii equation

$$i\hbar\frac{\partial\psi(z,t)}{\partial t}=\left(-\frac{\hbar^2}{2m_0}\frac{\partial^2}{\partial z^2}+V_{opt}(z)+g_{1D}|\psi(z,t)|^2\right)\psi(z,t) \tag{3}$$

where m_0 is the atomic mass and the renormalized 1D effective interaction g_{1D} is written in terms of the usual 3D scattering length a as [18]

$$g_{1D}=\frac{4\pi\hbar^2 a}{m_0}\int d^2\mathbf{x}_\perp|\psi_\perp(\mathbf{x}_\perp)|^4. \tag{4}$$

III. ALLOWED BANDS AND FORBIDDEN GAPS

As happens to electrons in crystalline solids [19] and light in periodic dielectric systems such as photonic band gap

crystals [6], the atomic dispersion in an infinite periodic potential is characterized in the linear regime (i.e., in the noninteracting case) by allowed bands and forbidden gaps.

When the depth V_0 of the lattice potential is weak with respect to the Bragg energy $\hbar\omega_{\rm Br}=\hbar^2k_{\rm Br}^2/2m_0$ the lowest part of the band structure can be accurately described within a *nearly-free-atom* approximation [16] in which only two coupled modes [7] are taken into account:

$$\psi(z)=a_f e^{ikz}+a_b e^{i(k-2k_{\rm Br})z}. \tag{5}$$

In this restricted (f,b) basis, the linear regime Hamiltonian has the following form:

$$H=\begin{pmatrix} \dfrac{\hbar^2k^2}{2m_0}+\dfrac{V_0}{2} & \dfrac{V_0}{4} \\ \dfrac{V_0}{4} & \dfrac{\hbar^2(k-2k_{\rm Br})^2}{2m_0}+\dfrac{V_0}{2} \end{pmatrix} \tag{6}$$

and the eigenenergies $\hbar\omega_{\pm}$ are equal to

$$\hbar\omega_{\pm}(k)=\hbar\omega_{\rm Br}+\frac{V_0}{2}+\hbar\omega_{\rm Br} \times\left[\left(\frac{\Delta k}{k_{\rm Br}}\right)^2\pm 2\sqrt{\left(\frac{\Delta k}{k_{\rm Br}}\right)^2+\left(\frac{V_0}{8\hbar\omega_{\rm Br}}\right)^2}\right], \tag{7}$$

where we have set $\Delta k=k-k_{\rm Br}$; the positive sign holds for the upper, conduction band and the minus sign for the lower, valence band. No states are present between $\omega_{\rm Br}+V_0/4$ and $\omega_{\rm Br}+3V_0/4$: this is the lowest forbidden gap in which the matter waves cannot propagate through the lattice.

The group velocity is given by

$$v_{\rm g}^{\pm}(k)=\frac{\partial\omega_{\pm}}{\partial k}=\frac{v_{\rm Br}\Delta k}{k_{\rm Br}}\left\{1\pm\left[\left(\frac{\Delta k}{k_{\rm Br}}\right)^2+\left(\frac{V_0}{8\hbar\omega_{\rm Br}}\right)^2\right]^{-1/2}\right\}; \tag{8}$$

close to a band edge ($\hbar v_{\rm Br}\Delta k\ll V_0$), the group velocity $v_{\rm g}^{\pm}$ is much reduced with respect to the Bragg velocity $v_{\rm Br}=\hbar k_{\rm Br}/m_0$; further away ($\hbar v_{\rm Br}\Delta k\gg V_0$), it recovers the free-space value $\hbar k/m$.

The effective mass of the atom is given by

$$\frac{1}{m_{\rm eff}(\Delta k)}=\frac{1}{\hbar}\frac{\partial^2\omega_{\pm}}{\partial k^2} =\frac{1}{m_0}\left\{1\pm\frac{8\hbar\omega_{\rm Br}}{V_0}\left[1+\left(\frac{\Delta k/k_{\rm Br}}{V_0/8\hbar\omega_{\rm Br}}\right)^2\right]^{-3/2}\right\}. \tag{9}$$

At the band edge ($\Delta k=0$), $m_{\rm eff}$ is much smaller in absolute value than the free-space atomic mass m_0; as usual, it is positive at the conduction band edge, while it is negative at the valence band edge. Further away from the band edge, $m_{\rm eff}$ coincides with the positive free-space value m_0 [19].

Around the band edge, the weights of the forward and backward traveling waves are comparable $|a_f|\simeq|a_b|$ for both valence and conduction bands: the density profile of the Bloch eigenfunction thus has a standing wave shape with a spatial period equal to the lattice period $l_{\rm Br}$. Further away from the gap, one component dominates the other: the Bloch eigenfunction then has a traveling wave character and the density profile is uniform over the unit cell of the lattice.

IV. PROPAGATION IN THE LINEAR REGIME

We now consider a coherent matter pulse (e.g., extracted from a Bose-Einstein condensate) which is moving along the waveguide with a uniform velocity v_0 close to the Bragg velocity $v_{\rm Br}$. Initially the atomic pulse is far outside the lattice. The initial density distribution of atoms in the cloud is taken as having a Gaussian shape:

$$\psi_{\rm inc}(z)=\psi_{\rm max}e^{ik_0z}e^{-(z-z_0)^2/2w_0^2}; \tag{10}$$

the carrier momentum is $\hbar k_0=m_0v_0$ and the carrier kinetic energy $\hbar\omega_0=\hbar^2k_0^2/2m_0$; since the wave packet is finite in space, its Fourier transform $\tilde{\psi}(k)$ has a finite momentum spread $\sigma_k=1/w_0$ around k_0. As for the lattice shape, we have checked that the qualitative features discussed in the present paper do not depend on the details of the incident pulse shape.

If the density is sufficiently low and the interactions sufficiently weak, the nonlinear term in the Gross-Pitaevskii equation (3) can be neglected and the time evolution of the matter field is accurately described by a linear Schrödinger equation. In this case, the superposition principle holds and the transmission of the pulse can be well described in momentum space in terms of the wave vector-dependent transmission amplitude $t(k)$:

$$\tilde{\psi}_{\rm t}(k)=t(k)\tilde{\psi}_{\rm inc}(k). \tag{11}$$

If the whole of the incident wave packet is contained in either a transmitting or a reflecting region of the spectrum [Fig. 2(a)], it will be transmitted [Fig. 2(b)] or reflected [Fig. 2(c)] without apparent reshaping. As discussed in full detail in previous papers [16], complete transmission occurs whenever propagating states are available at all spatial positions for the frequencies of interest. Given the smooth envelope of the lattice, interface reflections do not occur and the matter wave adiabatically follows the shape of the corresponding Bloch state; the typical sinusoidal shape of band edge Bloch wave functions [6,19] multiplying the broad pulse envelope can be clearly recognized while the wave packet is crossing the lattice [Fig. 2(b), inset]. On the other hand, if the wave packet frequency falls inside the forbidden gap at some spatial positions, the matter wave is not able to cross that region and is then nearly completely reflected back [Fig. 2(c)]; the inversion point is located at the beginning of the forbidden region, i.e., at the point at which the carrier frequency ω_0 enters the forbidden gap.

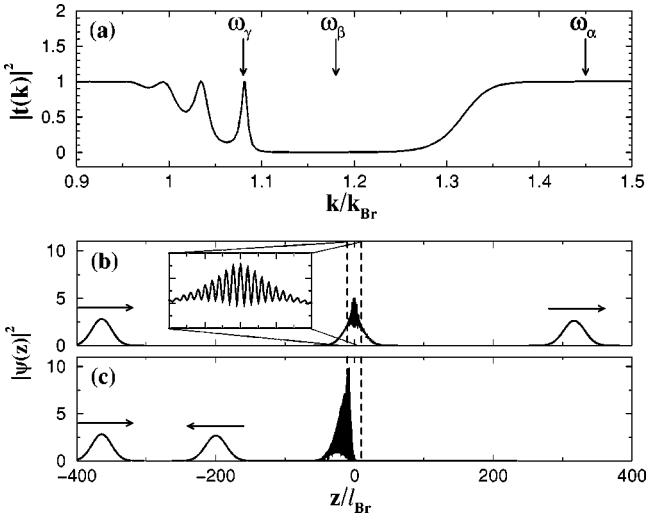

FIG. 2. (a) Linear transmission spectrum across a repulsive ($V_0/\omega_{Br}=1$) optical lattice with Gaussian profile ($w_l/l_{Br}=5$). Linear regime time evolution of Gaussian incident pulses ($w_0/l_{Br}=20$) centered at $\omega_0=\omega_\alpha$ (b) (transmitted) and $\omega_0=\omega_\beta$ (c) (reflected). The spatial extension of the lattice is indicated by the vertical dashed lines.

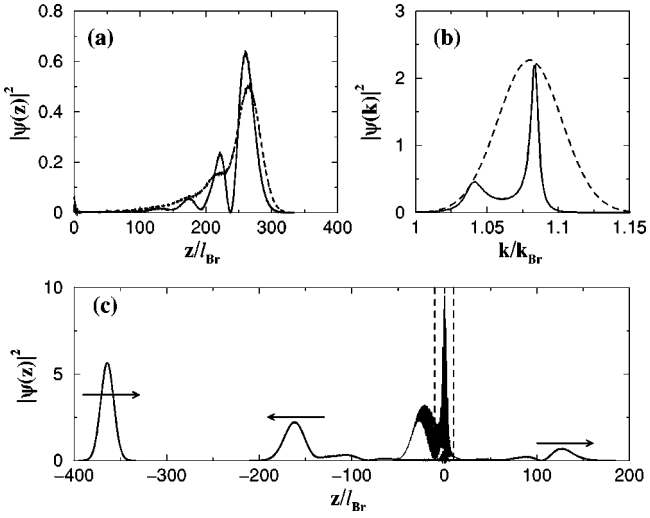

FIG. 3. (c) Time evolution of a weak and short ($w_0/l_{Br}=10$) Gaussian pulse close to resonance with a quasibound mode at $\omega_\gamma \simeq 1.17\omega_{Br}$ [see Fig. 2(a)]; lattice parameters as in Figs. 1 and 2. The spatial extension of the lattice ($w_l/l_{Br}=5$) is indicated by the vertical dashed lines. (a) Expanded view of the transmitted pulse shape for the pulse in (c) (solid line) and for a longer $w_0/l_{Br}=20$ pulse (dashed line); (b) incident (dashed) and transmitted (solid) spectra for the incident pulse in (c).

When one or more resonance peaks due to quasi-bound modes[1] are contained within the spectrum of the incident wave packet, the pulse will be partially reflected and partially transmitted [Figs. 3(b)–3(c)]; the strong frequency dependence of the transmission amplitude leads to a profound reshaping of the spatial profile of the pulse [Fig. 3(a)]. An incident pulse of linewidth much wider than the quasibound mode linewidth has in fact a time duration much shorter than the characteristic decay time of the mode; this latter can therefore be considered as being impulsively excited by the incident pulse and then exponentially decaying on a much longer time scale. The exponential tail shown by the transmitted pulse profile when a single quasibound mode is excited [dashed line in Fig. 3(a)] is a clear signature of transmission occurring via a single resonant quasibound mode [20].

If several isolated modes are instead present in the frequency interval encompassed by the incident spectrum, the spectrum of the transmitted pulse will contain several peaks [Fig. 3(b)] and a complex shape will result from the interference of the different frequency components. For example, if the incident pulse has a duration comparable to the dephasing time of a pair of neighboring modes (i.e., the inverse of their frequency difference), both of them will be impulsively excited and the profile of the transmitted pulse will show oscillations following the time evolution of the relative phase [solid line in Fig. 3(a)]; these oscillations can be interpreted as *quantum beatings* between the two coherently excited quasibound modes coupled to the same continuum of propagating modes outside the lattice.[2]

V. NONLINEAR REGIME AND MODULATIONAL INSTABILITY

For higher values of the atomic density and the coupling constant g_{1D}, the effect of the atom-atom interactions is no longer negligible and the mean-field nonlinear term $g_{1D}|\psi|^2$ in Eq. (3) starts playing an important role in the dynamics. In the following, we shall focus on the experimentally most relevant case of a positive scattering length $a>0$, which means a repulsive interaction among atoms in free space; furthermore, we shall limit ourselves to the case of a sufficiently weak nonlinearity $g_{1D}|\psi|^2 \ll V_0$ in order for the band structure of the atomic dispersion not to be washed out by the interaction term.

In [16] we discussed the case of a continuous wave (cw) beam of coherent atoms incident on a finite lattice; depending on the detuning of the incident beam with respect to the frequency of a quasibound mode of the lattice, atom-optical limiting or bistability was predicted for an incident beam respectively on or above the resonance frequency. Here we shall consider the more realistic case of a finite atomic wave packet incident on a finite optical lattice; its central frequency ω_0 is taken to be close to that of a quasibound mode of the lattice and its temporal duration much longer than the lifetime of the mode so that the frequency spread is narrower than the mode linewidth.

[1]In analogy with optics, these quasibound modes correspond to the resonance peaks of a Fabry-Pérot interferometer or, more closely, to the cavity modes of a distributed Bragg reflector (DBR) microcavity [6(b)]. A more detailed discussion about quasibound modes in optical lattices can be found in [16] and in [14,15].

[2]Similar oscillations were studied in [15] in the case in which a large number of closely spaced quasibound modes are excited.

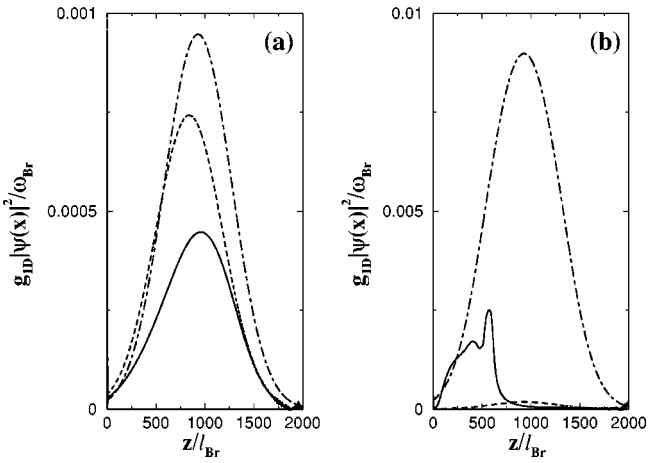

FIG. 4. Transmitted pulse shape for Gaussian incident pulses on resonance (a) and $0.04\omega_{\mathrm{Br}}$ above resonance (b) with the quasibound mode of the lattice at $\omega_\gamma \simeq 1.17\omega_{\mathrm{Br}}$ (solid lines). For comparison, same calculations neglecting the interaction term (dashed lines) and in the absence of the lattice (dot-dashed lines) are shown. Same lattice parameters as in Figs. 2 and 3; the pulse starts at $z_0/l_{\mathrm{Br}} = -1000$ with a Gaussian width equal to $w_0/l_{\mathrm{Br}} = 480$.

First we consider the case of an incident wave packet with a center-of-mass kinetic energy $\hbar\omega_0$ exactly on resonance with a quasibound mode [Fig. 4(a)]: in the absence of interactions (dashed line), the wave packet is nearly completely transmitted without any shape distortion; only a small fraction of the pulse is reflected [Fig. 5(a)]. Thanks to the resonance condition with the quasibound mode, the atomic density inside the lattice is significantly larger than that in the incident wave packet. In the presence of interactions, the main effect of nonlinearity is to blueshift the quasibound mode frequency [11] and push it out of resonance with the incident beam; this negative feedback effect, already present in the cw treatment [16], gives not only a saturation of the transmission as a function of the incident density (*atom-optical limiting*), but also a significant reshaping of the wave packet: the higher density part is cut and the resulting wave packet is flattened. The negative feedback in the transmission obviously corresponds to a positive feedback in the reflection.

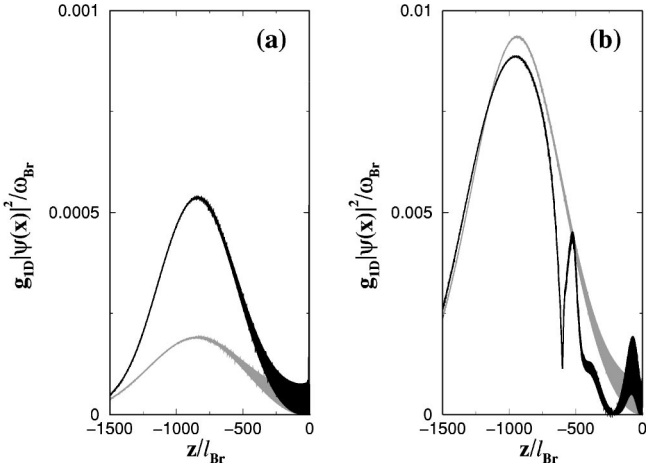

FIG. 5. Reflected pulse shapes for the same values of the physical parameters as in Fig. 4 (black lines): (a) refers to the resonant case, and (b) to the off-resonant case. For comparison, same calculation neglecting the interaction term is shown (gray lines).

In the opposite case of a wave packet incident with a kinetic energy higher than the quasimode frequency, a low density wave packet is nearly completely reflected [Fig. 4(b), dashed line]. At higher densities, the cw calculations in [16] predicted the appearance of *atom-optical bistability* effects: several stationary states with different transmitted intensities can indeed be found for the same value of the incident intensity. On such grounds, we are able to put forward a physical interpretation of the transmitted pulse shape in the presence of interactions shown as a solid line in Fig. 4(b): only a small fraction of the leading part of the pulse is transmitted since the incident frequency is out of resonance with the empty quasibound mode; moreover, this part of the incident wave packet has been accelerated by the repulsive mean-field interactions before reaching the lattice and thus pushed even further off resonance.[3] For the same reason, the trailing part of the pulse has been slowed down with respect to the central velocity and thus is closer to resonance with the quasibound mode; when this trailing part of the pulse reaches the lattice, the quasibound mode starts to be effectively populated. The main effect of the interactions among the atoms in the quasibound mode is to push its frequency closer to resonance with the incident wave packet: the sudden increase in the density of the transmitted pulse that is apparent in Fig. 4(b) is a direct consequence of this positive feedback. This behavior is analogous to the jump from the lower to the upper branch of the bistability loop that occurs in the cw case for incident intensities growing beyond the switch-on threshold. The shape of the reflected pulse is complementary to that of the transmitted pulse: in the presence of the nonlinearity, the reflected pulse shows a dip corresponding to the switch-on of the transmission [Fig. 5(b)].

Provided the interaction energy is much smaller than the spacing of the different quasibound modes, the transmission dynamics is mostly determined by a single resonant mode and the shape of the matter field inside the lattice is fixed by the eigenfunction of the mode; this guarantees that no *modulational instability* can occur[4] even in the presence of an effectively attractive interaction such as the one which occurs in the case of negative mass $m_{\mathrm{eff}} < 0$ valence band atoms

[3]In the previous case [Fig. 4(a)] this acceleration effect was not apparent since the nonlinearity required to observe the optical limiting effect is generally weaker than the one required for optical bistability.

[4]From a different point of view, this suppression of the modulational instability can be interpreted in the following terms: If the spatial extension of the condensate wave packet is small enough, the excitation of the long wavelength modes that are responsible for the modulational instability cannot occur because of the finite size of the system; this effect is well known from the physics of trapped BECs with attractive interactions, which are stable provided the number of atoms is sufficiently small for the effective healing length to be larger than the condensate size [21,22].

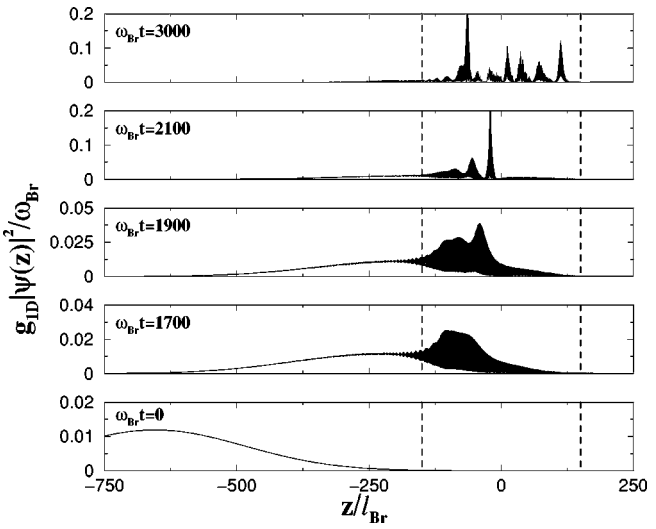

FIG. 6. Onset of modulational instability: propagation of a pulse of valence band atoms ($\omega_0/\omega_{Br}=0.68$, $w_0/l_{Br}=240$, $z_0/l_{Br}=-650$) across an attractive lattice ($V_0/\omega_{Br}=-0.4$). The lattice has a flat profile in the central $|z/l_{Br}|<100$ region and Gaussian ($w_l/l_{Br}=50$) wings; its spatial extension is indicated by the vertical dashed lines.

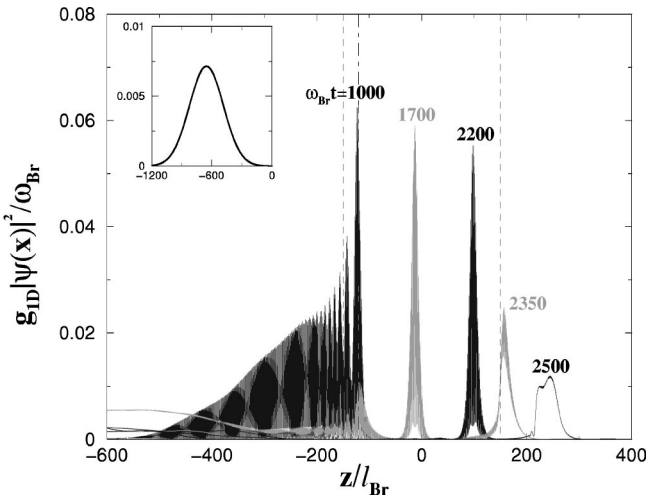

FIG. 7. Bright-gap-soliton generation from a standing matter wave (same lattice parameters as in Fig. 6): pulse shape snapshots at different times. Vertical dashed lines indicate the spatial extension of the lattice; the dot-dashed line indicates the reflection point in the linear regime. Inset: incident pulse profile ($\omega_0/\omega_{Br}=0.72$, $w_0/l_{Br}=240$, $z_0/l_{Br}=-650$).

for which the sign of the effective interaction is reversed with respect to free space.

On the other hand, a spatially extended wave packet of coherent valence band atoms in the absence of spatial confinement is instead subjected to modulational instability: consider, for example, an attractive lattice and an incident wave packet with a kinetic energy just below the lower edge of the gap. Since propagating valence band states are available at all spatial positions, the pulse is able to penetrate inside the lattice without any reflection. As soon as the pulse is in the lattice, the initially smooth envelope starts being modulated with an amplitude that grows exponentially in time and, at the end, a train of narrow and intense pulses is found (Fig. 6). The seed for this modulational instability is automatically provided by the density modulations which inevitably arise while the pulse is entering the nonuniform lattice.

In Fig. 6 a very idealized lattice shape with a flat central part and Gaussian wings has been considered; we have, however, checked that the qualitative features remain unchanged if different lattice or pulse shapes are taken into consideration.

A similar modulational instability is well known to occur in nonlinear Bragg fiber optics [7]; a cw laser beam traveling in the conduction (valence) photonic band of a Bragg lattice with a focusing (defocusing) nonlinear refractive index is subjected to self-pulsation and therefore converted into a train of pulses. Since the nonlinear refractive index can be interpreted as an effective photon-photon interaction [23,24], this self-pulsing effect is easily explained as arising from the modulational instability due to the effective attractive interaction.

VI. BRIGHT-GAP-SOLITON GENERATION

A regular train of short optical pulses with a well-defined period and intensity has been theoretically shown to be produced if the modulational instability of a cw laser beam propagating in a lattice is seeded with a weak periodic intensity modulation [10]. The shape of each pulse is stable during propagation since the group velocity dispersion is counterbalanced by the optical nonlinearity. Following the literature, we shall call these pulses *gap solitons* [7], even if from a strictly mathematical point of view they could be classified only as solitary waves, since the wave equation (3) in a periodic potential is not exactly integrable [23] and collisions between two such solitons do not exactly preserve the pulse shape [25]; as we shall see in the following, the expression ''gap soliton'' is, however, physically justified by the fact that the pulse distortion following a collision is generally small. Since the first observation of optical gap solitons in 1995, intense experimental activity has occurred for the generation and characterization of gap solitons and Bragg modulational instabilities in optical fibers [9].

In very recent years, solitonic excitations are also beginning to be investigated in the context of nonlinear atom optics [18]: dark solitons in the form of stable density dips in an otherwise uniform condensate have been recently observed [26]; bright gap solitons [4] and modulational instabilities [5] are actually under intense investigation; despite the positive atom-atom scattering length, such stable atomic pulses can exist inside an optical lattice thanks to the negative effective mass of valence band atoms. In the present section we present a method to generate narrow bright gap solitons starting from a wide atomic condensate incident on an optical lattice

Consider a long coherent matter wave pulse (i.e., a Bose-condensed atomic cloud) incident on the same attractive lattice as in the previous section but with a kinetic energy just above the lower edge of the gap. In the linear regime, such a wave packet is nearly completely reflected so that the interference of the incident and reflected waves creates a standing wave pattern in front of the reflection point. Far outside the

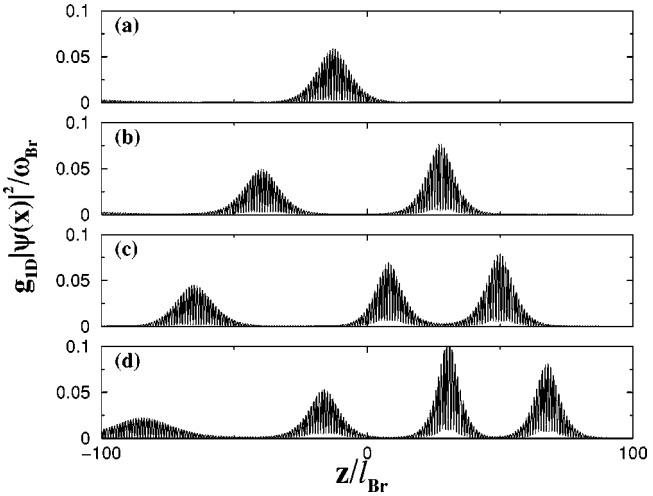

FIG. 8. Dependence of bright-soliton number and properties on the interaction parameter g_{1D}. In (a) the lattice and incident pulse parameters are the same as in Fig. 7; in (b), (c), and (d) the densities of the incident pulse are a factor of, respectively, 4/3, 5/3, and 2 larger than in (a). All snapshots are take at the same time $\omega_{Br}t = 1700$.

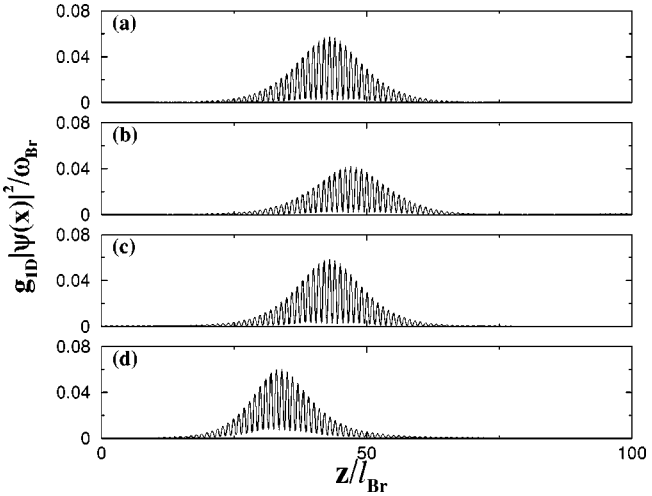

FIG. 9. Bright-soliton generation for different pulse and lattice shapes. In (a) and (b) the lattice is the same Gaussian-flat lattice as in Figs. 6–8; in (a) the incident pulse is Gaussian ($w_0/l_{Br}=240$), while in (b) it has an inverted parabolic (Thomas-Fermi) shape. In (c) a Gaussian pulse ($w_0/l_{Br}=240$) is incident on a lattice with a flat central region for $|z/l_{Br}|<100$ and Lorentzian edges of characteristic width $w_l/l_{Br}=50$. In (d) a Gaussian pulse ($w_0/l_{Br}=160$) is incident on a Gaussian lattice ($w_l/l_{Br}=100$).

lattice, the period of the pattern is fixed by the wave vector k_0 of the incident wave packet and is therefore of the order of the lattice period l_{Br}. Inside the lattice, the standing wave pattern originates instead from the interference of a forward and a backward Bloch wave: the amplitude of the fast oscillations follows from the density modulation of each Bloch wave function with a periodicity l_{Br}, while the local period of the slower modulation that originates from the interference of the two Bloch waves at $k=k_{Br}\pm\Delta k$ is equal to $2\pi/\Delta k$. As we approach the reflection point, the Bloch waves approach the band edge, so that $\Delta k\rightarrow 0$ and the period of the modulation is strongly increased with respect to the lattice period, although it still remains much shorter than the size of the incident condensate; this effect is apparent in the leftmost snapshot of Fig. 7. Provided the nonlinear term is sufficiently small, the interactions do not wash out the standing wave interference pattern [27] but simply blueshift the local band edge at the spatial position of the rightmost antinodes; in this way, the wave packet frequency is pushed out from the local gap and valence band states become available for propagation. The resulting short pulses, stabilized by the effective attractive interaction, can therefore propagate along the lattice as solitonic objects. The stronger the nonlinear term, the larger the number of pulses for which this mechanism is effective and which are then able to propagate along the whole lattice without being reflected; as shown in Fig. 7, a parameter range can be found in which a single soliton is generated. In Fig. 8 we have plotted the shape of the solitonic pulse train for different values of the density: the higher the density, the larger the number of solitons forming the train; in the presence of several solitons, the dynamics can be complicated by oscillations and mass exchange effects between the different pulses. For lower densities, the linear regime is recovered and the incident pulse is nearly completely reflected. In Figs. 7 and 8, a lattice with Gaussian edges and a central flat region was used: in this way, after the initial complex nucleation stage at the front edge of the lattice, the dynamics is made simple by the fact that the solitons freely propagate through a uniform periodic lattice.

In Figs. 9(a)–9(c), we illustrate how the generation of a solitonic pulse relies on neither the specific Gaussian shape of the incident pulse, nor the Gaussian shape of the lattice edges: a calculation similar to the ones of Figs. 7 and 8 has been repeated for different incident pulse and lattice shapes and in all cases, provided the density in the incident pulse is carefully tuned, it was possible to obtain a single solitonic pulse. As a further check, we verified that a soliton can also

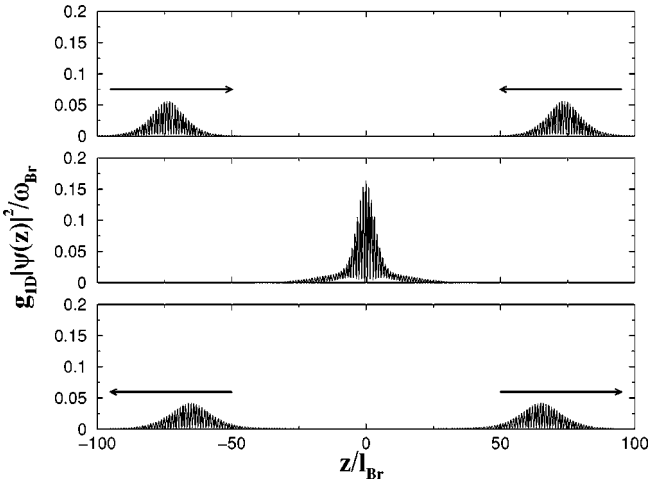

FIG. 10. Collision process between a pair of gap solitons generated at either end of a lattice with the same parameters as in Fig. 7 and propagating along the lattice with opposite velocities. All the collisional dynamics take place in the region $|z/l_{Br}|<100$ where the lattice profile is flat.

be generated using a simple Gaussian lattice without a flat region [Fig. 9(d)]: in this case the dynamics is more complex, however, since the lattice parameters are spatially varying. The center-of-mass motion is no longer uniform and the pulse width changes because of the spatially varying effective mass.

In summary, we have found that the generation of a single bright-gap soliton from a wide condensate is a rather robust feature with respect to changes in the initial parameters; however, given the complexity of the nucleation process, it is not physically evident how to control the parameters of the soliton such as velocity and peak density by acting on the parameters of the lattice and of the incident pulse.

Once the pulse has crossed the lattice and has got to its opposite end, the effective mass of the atoms becomes positive again and the pulse is immediately broadened under the combined effect of group velocity dispersion and mean-field repulsion (see the two last snapshots in Fig. 7). A proof of the solitonic nature of the generated pulse is obtained from a study of its collisional dynamics (Fig. 10): a pair of such pulses symmetrically generated at the two ends of the lattice collide in the middle of the lattice. Their solitonic properties result clearly from the fact that their shapes as well as the number of atoms contained in each of them are only weakly affected by the collision process. The small broadening of the pulses that can be observed in Fig. 10 is a signature of the fact that the nonlinear wave equation in a periodic potential is integrable only in an approximate way [25,28].

Because the effective mass $m_{\rm eff}$ is much smaller than the free-space mass m_0 (for the parameters of Fig. 7 $m_{\rm eff}=-0.07m_0$), the solitonic width is significantly larger than the free-space healing length at the same value of the density; for a typical value of the lattice period of the order of 0.5 μm, the solitonic length turns out of the order of 10 μm, which is well within the capabilities of actual detection systems. The mean-field interaction energies required for the observation of solitonic effects are in general smaller than or of the order of one-tenth of the recoil energy $\omega_{\rm Br}$: for the most relevant case of ^{87}Rb atoms and ^{23}Na, the recoil energy corresponds to reasonable densities of the order of 10^{14} cm^{-3}. The characteristic time for the modulational instability and soliton formation processes described in the previous sections is of the order of $\omega_{\rm Br}t\simeq 500$, which means $t\simeq 20$ ms for ^{23}Rb atoms and $t\simeq 3$ ms for ^{87}Na.

The method here described for the generation of bright gap solitons is significantly different from previous proposals [4]: in our approach the soliton pulse shape originates not from the whole BEC cloud, but only from the much shorter density bump corresponding to an antinode of the standing matter wave. This fact allows one to obtain short solitons from a wide BEC without the need for a dramatic pulse compression under the effect of effectively attractive interactions.

VII. GAP SOLITONS: A SIMPLE ANALYTICAL MODEL

Provided the gap soliton is wide enough, only a narrow group of Bloch states around a central wave vector $k_{\rm sol}$ are populated and an accurate description can be analytically obtained within the so-called envelope-function framework. Denoting by $u_{k_{\rm sol}}(z)$ the Bloch eigenfunction at $k=k_{\rm sol}$, we write the wave function $\psi(z,t)$ of the coherent matter pulse as the product of the slowly varying envelope $\overline{\psi}(z,t)$ and the quickly oscillating Bloch eigenfunction $u_{k_{\rm sol}}(z)$:

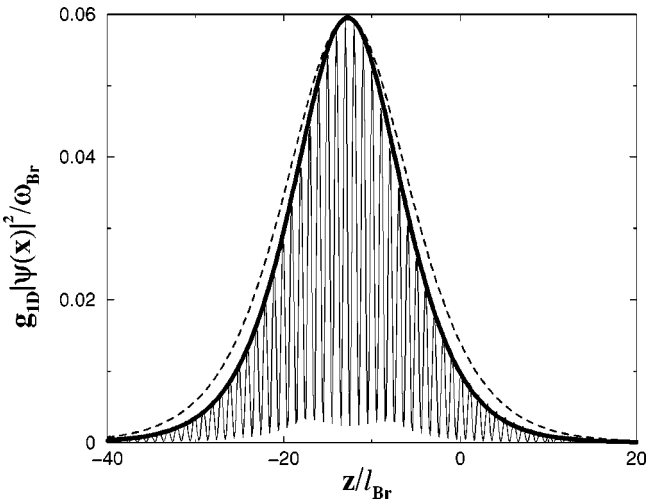

FIG. 11. Comparison of the numerically calculated solitonic pulse at $\omega_{\rm Br}t=1700$ in Fig. 7 (thin solid line) with the analytical prediction (18) for the envelope (thick solid line). Dashed line: approximate prediction obtained using the band edge values ($k_{\rm sol}=k_{\rm Br}$) for $g_{\rm eff}$ and $m_{\rm eff}$.

$$\psi(z,t)=\overline{\psi}(z,t)u_{k_{\rm sol}}(z); \tag{12}$$

in the following, the Bloch eigenfunction $u_k(z)$ is assumed to be normalized according to

$$\frac{1}{l_{\rm Br}}\int_0^{l_{\rm Br}} dz|u_k(z)|^2=1, \tag{13}$$

which corresponds to

$$|a_f|^2+|a_b|^2=1, \tag{14}$$

in the (f,b) basis of Eq. (5). If the variations of the envelope $\overline{\psi}(z,t)$ are slow enough, it can be shown [28] that $\overline{\psi}(z,t)$ obeys a simple integrable nonlinear Schrödinger equation

$$i\hbar\frac{\partial\overline{\psi}(z,t)}{\partial t}=\left(-\frac{\hbar^2}{2m_{\rm eff}}\frac{\partial^2}{\partial z^2}+g_{\rm eff}|\overline{\psi}(z,t)|^2\right)\overline{\psi}(z,t), \tag{15}$$

in which the effective mass $m_{\rm eff}$ and the effective coupling $g_{\rm eff}$ depend on the central wave vector $k_{\rm sol}$. While an explicit expression for $m_{\rm eff}(k)$ has already been given in Eq. (9), the effective coupling $g_{\rm eff}(k)$ turns out to be expressed in terms of the Bloch wave function by

$$g_{\rm eff}(k)=\frac{1}{l_{\rm Br}}\int_0^{l_{\rm Br}} dz g_{1D}|u_k(z)|^4; \tag{16}$$

obviously, the sign of $g_{\rm eff}$ is always the same as that of $g_{\rm 1D}$, which, in the case we are considering, means $g_{\rm eff}>0$. Within the two-mode ansatz, Eq. (5), this quantity can be rewritten in the simple form

$$g_{\rm eff}(k)=g_{\rm 1D}(|a_f|^4+|a_b|^4+4|a_f|^2|a_b|^2), \tag{17}$$

where $a_{f,b}$ are the projections of the Bloch eigenfunction on the forward and backward propagating waves. Notice that the density modulation of the Bloch wave function at the gap edge ($|a_f|^2=|a_b|^2=1/2$) makes the effective coupling a factor of 3/2 larger than that far from the gap, i.e., the free-space coupling.

Under these assumptions, the envelope $\overline{\psi}_{\rm sol}$ of the solitonic wave packet has the simple expression [23]

$$\overline{\psi}_{\rm sol}(z)=\overline{\psi}_{\rm max}\,{\rm sech}\left(\frac{z-v_g t}{\xi_{\rm sol}}\right), \tag{18}$$

with the width $\xi_{\rm sol}$ given by

$$\xi_{\rm sol}=\sqrt{\frac{\hbar^2}{|m_{\rm eff}|g_{\rm eff}|\overline{\psi}_{\rm max}|^2}}; \tag{19}$$

as expected, the size $\xi_{\rm sol}$ of the soliton is of the order of the healing length $\xi=\hbar/\sqrt{2|m_{\rm eff}|g_{\rm eff}|\overline{\psi}_{\rm max}|^2}$. The accuracy of this approximate description is apparent in Fig. 11 where we compare the numerically obtained wave packet with the analytical prediction (18) for the envelope; the central wave vector $k_{\rm sol}$ of the wave packet was determined from the group velocity by means of Eq. (8), the envelope amplitude $\overline{\psi}_{\rm max}$ from the peak density of the pulse.

VIII. CONCLUSIONS

In this paper we have theoretically investigated the transmission dynamics of coherent matter pulses (such as those that can be extracted from Bose-Einstein condensates) which are incident on finite optical lattices; such systems are matter wave analogs of the nonlinear Bragg fibers currently studied in nonlinear optics.

In the linear regime (i.e., in the low-density or weak-interaction limit), we have characterized the dependence of the intensity and shape of the transmitted pulse on the velocity and size of the incident condensate in terms of the dispersion of matter waves inside the lattice; as in the case of light waves in periodic dielectric structures or in the case of electrons in crystalline solids, the dispersion of matter waves in the periodic potential of optical lattices is in fact characterized by allowed bands and forbidden gaps.

The dynamics in the presence of interactions is found to be even richer: an interpretation of the numerically predicted effects is put forward in terms of familiar concepts from nonlinear optics, such as optical limiting, optical bistability, and modulational instability.

In particular, we have investigated a possible way of generating narrow bright gap solitons from a wide incident Bose condensate: the modulational instability is seeded from the strongly inhomogeneous density profile of the standing wave that is formed in front of the finite optical lattice by the interference of the incident and reflected matter waves. The solitonic nature of the generated pulses has been checked from their shape, which is in excellent agreement with a simple analytical model, as well as from their dynamical and collisional properties.

Finally, we have verified that the range of physical parameters that is required for the observation of the effects predicted in the present paper falls well within the possibilities of actual experimental setups.

ACKNOWLEDGMENTS

Financial support from the INFM grant PRA-PHOTONMATTER is acknowledged. I.C. acknowledges financial support from the EU (''Improving Human Research Potential and the Socio-economic Knowledge Base'' under Contract No. HPMF-CT-2000-00901). I.C. is grateful to Yvan Castin, Lincoln Carr, and Anna Minguzzi for useful discussions. Laboratoire Kastler Brossel is a Unité de Recherche de l'Ecole Normale Supérieure et de l'Université Paris 6, associée au CNRS.

[1] C.S. Adams and E. Riis, Prog. Quantum Electron. **21**, 1 (1997); E. Peik, M. Ben Dahan, I. Bouchoule, Y. Castin, and C. Salomon Phys. Rev. A **55**, 2989 (1997); Q. Niu, X.-G. Zhao, G.A. Georgakis, and M.G. Raizen, Phys. Rev. Lett. **76**, 4504 (1996); S.R. Wilkinson, C.F. Bharucha, K.W. Madison, Q. Niu, and M.G. Raizen, *ibid.* **76**, 4512 (1996).

[2] *Bose-Einstein Condensation in Atomic Gases*, Proceedings of the International School of Physics ''Enrico Fermi,'' Course CXL, edited by M. Inguscio, S. Stringari, and C. Wieman (IOS Press, Amsterdam, 1999).

[3] B.P. Anderson and M. Kasevich, Science **282**, 1686 (1998); S. Burger *et al.*, Phys. Rev. Lett. **86**, 4447 (2001); O. Morsch, J.H. Müller, M. Cristiani, D. Ciampini, and E. Arimondo, *ibid.* **87**, 140402 (2001); M. Greiner, I. Bloch, O. Mandel, T.W. Hänsch, and T. Esslinger, *ibid.* **87**, 160405 (2001).

[4] O. Zobay, S. Pötting, P. Meystre, and E.M. Wright, Phys. Rev. A **59**, 643 (1999); S. Pötting, O. Zobay, P. Meystre, and E.M. Wright, J. Mod. Opt. **47**, 2653 (2000); A. Trombettoni and A. Smerzi, Phys. Rev. Lett. **86**, 2353 (2001).

[5] B. Wu and Q. Niu, Phys. Rev. A **64**, 061603 (2001); V.V. Konotop and M. Salerno, *ibid.* **65**, 021602 (2002); F.Kh. Abdullaev *et al.*, *ibid.* **65**, 021602 (2002).

[6] (a) E. Yablonovitch, J. Phys.: Condens. Matter **5**, 2443 (1993); (b) *Confined Electrons and Photons*, edited by E. Burstein and C. Weisbuch (Plenum Press, New York, 1995).

[7] C. M. de Sterke and J. E. Sipe, in *Progress in Optics XXXIII*, edited by E. Wolf (Elsevier Science, Amsterdam, 1994), p. 203.

[8] K. Berg-Sorensen and K. Molmer, Phys. Rev. A **58**, 1480 (1998); D. Jaksch, C. Bruder, J.I. Cirac, C.W. Gardiner, and P. Zoller, Phys. Rev. Lett. **81**, 3108 (1998); S. Potting, M. Cramer, C.H. Schwalb, H. Pu, and P. Meystre, Phys. Rev. A **64**, 023604 (2001).

[9] B.J. Eggleton, R.E. Slusher, C.M. de Sterke, P.A. Krug, and J.E. Sipe, Phys. Rev. Lett. **76**, 1627 (1996); B.J. Eggleton, C.M. de Sterke, and R.E. Slusher, J. Opt. Soc. Am. B **16**, 587 (1999); S. Pitois, M. Haelterman, and G. Millot, Opt. Lett. **26**, 780 (2001).

[10] C.M. de Sterke and J.E. Sipe, Phys. Rev. A **42**, 2858 (1990); C.M. de Sterke, *ibid.* **45**, 8252 (1992); H.G. Winful, R. Zamir, and S. Feldman, Appl. Phys. Lett. **58**, 1001 (1991); C.M. de Sterke, Phys. Rev. A **45**, 8252 (1992); A.B. Aceves, C. de Angelis, and S. Wabnitz, Opt. Lett. **17**, 1566 (1992); N.M. Litchinitser, G.P. Agrawal, B.J. Eggleton, and G. Lenz, Opt. Express **3**, 411 (1998).

[11] R.W. Boyd, *Nonlinear Optics* (Academic Press, London, 1992); P.N. Butcher and D. Cotter, *The Elements of Nonlinear Optics* (Cambridge University Press, Cambridge, England, 1993).

[12] N. Friedman, R. Ozeri, and N. Davidson, J. Opt. Soc. Am. B **15**, 1749 (1998).

[13] L. Santos and L. Roso, Phys. Rev. A **57**, 432 (1998).

[14] L. Santos and L. Roso, Phys. Rev. A **58**, 2407 (1998).

[15] L. Santos and L. Roso, Phys. Rev. A **60**, 2312 (1999).

[16] I. Carusotto and G.C. La Rocca, Phys. Rev. Lett. **84**, 399 (2000); in *Bose-Einstein Condensates and Atom Lasers*, edited by S. Martellucci, A.N. Chester, A. Aspect, and M. Inguscio (Kluwer Academic/Plenum Publishers, New York, 2000), p. 153.

[17] K. Bongs *et al.*, Phys. Rev. A **63**, 031602 (2001); A. Görlitz *et al.*, Phys. Rev. Lett. **87**, 130402 (2001); F. Schreck *et al.*, *ibid.* **87**, 080403 (2001).

[18] W.P. Reinhardt and C.W. Clark, J. Phys. B **30**, L785 (1997); A.D. Jackson, G.M. Kavoulakis, and C.J. Pethick, Phys. Rev. A **58**, 2417 (1998); Th. Busch and J.R. Anglin, Phys. Rev. Lett. **84**, 2298 (2000); Th. Busch and J.R. Anglin, *ibid.* **87**, 010401 (2001).

[19] N.W. Ashcroft and N.D. Mermin, *Solid State Physics* (Saunders College Publishing, Orlando, FL, 1976).

[20] C. Cohen-Tannoudji, J. Dupont-Roc, and G. Grynberg, *Processus d'Interaction entre Photons et Atomes* (InterEditions/ Editions du CNRS, Paris, 1988), exercise 13.

[21] P.A. Ruprecht, M.J. Holland, K. Burnett, and M. Edwards, Phys. Rev. A **51**, 4704 (1995); Yu. Kagan, G.V. Shlyapnikov, and J.T.M. Walraven, Phys. Rev. Lett. **76**, 2670 (1996).

[22] C.A. Sackett, H.T.C. Stoof, and R.G. Hulet, Phys. Rev. Lett. **80**, 2031 (1998).

[23] *Optical Solitons*, edited by J.R. Taylor (Cambridge University Press, Cambridge, England, 1992).

[24] I.H. Deutsch, R.Y. Chiao, and J.C. Garrison, Phys. Rev. A **47**, 3330 (1993).

[25] A.B. Aceves and S. Wabnitz, Phys. Lett. A **141**, 37 (1989).

[26] S. Burger *et al.*, Phys. Rev. Lett. **83**, 5198 (1999); J. Denschlag *et al.*, Science **287**, 97 (2000).

[27] L.D. Carr, C.W. Clark, and W.P. Reinhardt, Phys. Rev. A **62**, 063610 (2000); W.-M. Liu, B. Wu, and Q. Niu, Phys. Rev. Lett. **84**, 2294 (2000).

[28] C.M. de Sterke and J.E. Sipe, Phys. Rev. A **42**, 550 (1990); C.M. de Sterke and B.J. Eggleton, Phys. Rev. E **59**, 1267 (1999).